crystals

MDPI

Article

A Novel Halogen Bond Acceptor: 1-(4-Pyridyl)-4-Thiopyridine (PTP) Zwitterion

Xin Ding, Matti Tuikka and Matti Haukka *

Department of Chemistry, University of Jyväskylä, P.O. Box 35, FI-40014 Jyväskylä, Finland; xin.x.ding@jyu.fi (X.D.); MTU@dinex.fi (M.T.)

* Correspondence: matti.o.haukka@jyu.fi ; Tel.: +358-40-8054666

Received: 7 February 2020; Accepted: 29 February 2020; Published: 3 March 2020

Abstract: Sulfur is a widely used halogen bond (XB) acceptor, but only a limited number of neutral XB acceptors with bifurcated sp^3-S sites have been reported. In this work a new bidentate XB acceptor, 1-(4-pyridyl)-4-thiopyridine (PTP), which combines sp^3-S and sp^2-N acceptor sites, is introduced. Three halogen bonded cocrystals were obtained by using 1,4-diiodobenzene (DIB), 1,4-diiodotetrafluorobenzene (DIFB), and iodopentafluorobenzene (IPFB) as XB donors and PTP as acceptor. The structures of the cocrystals showed some XB selectivity between the S and N donors in PTP. However, the limited contribution of XB to the overall molecular packing in these three cocrystals and the results from DSC measurements clearly point out the synergetic influence and interplay of all noncovalent interactions in crystal packing of these compounds.

Keywords: Halogen bonds (XB); acceptor; cocrystals; selectivity

1. Introduction

Halogen bond (XB) is a noncovalent interaction occurring between an electrophilic region (σ-hole) of a halogen atom (XB donor) in a molecular moiety and a nucleophilic atom (XB acceptor) in the same or another moiety [1]. The major force in XB is electrostatic by nature [2], but charge transfer, polarization, and dispersion forces all play important roles in XB contacts [3,4]. The strength of a typical XB is comparable with the hydrogen bonds (HB) and in some cases is even stronger than HB [5]. Just like the hydrogen bond, XB is also highly directional [6–8]. Due to these characteristics, XB has emerged as a prominent tool in crystal engineering [9–13], organic synthesis [14,15], and biochemistry [16,17], etc.

Commonly used XB acceptors include sp^2 oxygen atoms (sp^2-O) [18,19], sp^3 oxygen atoms (sp^3-O) [20–22], sp^2 sulfur atoms (sp^2-S) [23–26], sp^3 sulfur atoms (sp^3-S) [27–29], and sp^2 nitrogen atoms (sp^2-N) [30–34]. Unlike the sp^2-N, both sp^2-S and sp^3-S can act as bifurcated XB acceptors in three-centered halogen bonds, due to the two available lone pairs on sulfur [9]. Similarly, both sp^2-O and sp^3-O can function as multidentate XB acceptors. However, a CCDC survey (C-X···S, C-X···O, X=Br, I; no organometallic complexes; CSD version 5.41, November 2019) gave 539 structures with C-X···S, of which 403 have sp^3-S as the XB acceptor, but only 20 structures include bifurcated sp^3-S. Eight of these structures involve SCN^- and 10 C-S-C synthon as the XB acceptor. Altogether 4799 structures with C-X···O were found in the CCDC survey with 1249 sp^3-O as the XB acceptor. However, only 39 structures have multidentate sp^3-O, of which 24 are N-O synthons and 12 are C-O synthons. Clearly, compared with the oxygen atom as XB acceptor, the sulfur atom is less commonly studied.

Thus, our aim was to develop a new neutral bidentate S-N-type XB acceptor capable of forming three-centered XBs via S and two-centered XBs through N. PTP, in Figure 1, was synthesized for such purpose. Unlike in the C-S-C synthon, the sp^3-S pendant in PTP is not sterically hindered and the sp^2-N at the other end of the PTP molecule assures the 1:1 ratio interaction with XB donors. Since

the PTP is a neutral zwitterionic molecule, it is possible to avoid introducing any undesirable cations into the system. I_2 is the simplest bidentate XB donor, which can be used to link organic molecules together via XB [35–40]. However, I_2 is not always the most ideal linker due to its redox properties, which easily lead to unwanted side reactions. Therefore, we chose less redox active organic iodides—1,4-diiodobenzene (DIB) and 1,4-diiodotetrafluorobenzene (DITFB) as the bidentate and iodopentafluorobenzene (IPFB) as monodentate XB donors—in this work (Figure 1).

The ultimate goal of this study was to investigate the ability of PTP to form robust supramolecular structures via XB interactions. Furthermore, the possible preferences between the S and N acceptors in XB formation were also investigated.

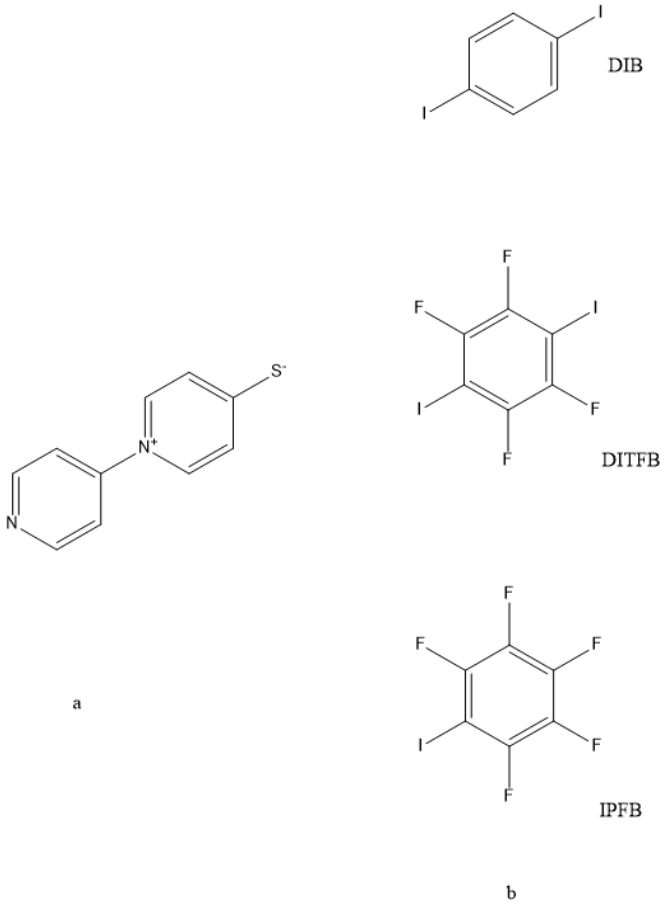

Figure 1. Schematic structure of XB acceptor and donors. **(a)** The schematic structure of PTP; **(b)** the schematic structure of 1,4-diiodobenzene (DIB), of 1,4-diiodotetrafluorobenzene (DITFB), and of iodopentafluorobenzene (IPFB).

2. Materials and Methods

Materials. 4-Mercaptopyridine (95%), sodium hydroxide (98%), DIB (99%), DITFB (98%), and IPFB (99%) were from Sigma-Aldrich. Dichloromethane (99%) and acetonitrile (99.8%) were obtained from VWR Chemicals. Silica-gel 60 (0.04–0.06 mm) was received from Merck. All reagents were used as received.

Solution Crystallization. Crystals of PTP were obtained by slowly evaporating the solution of 5 mg PTP + XB donor dissolved in 6 mL DCM at room temperature. The impact of the PTP/XB donor ratio on the cocrystal formation was studied using solutions with molar ratios of 1:1, 1:2, and 1:4 (PTP:XB donor). The X-ray quality crystals were typically obtained in 3 to 7 days when the solution was evaporated until crystals formed, but not completely dry. Analysis of all crystals obtained showed that the 1:1 ratio only yielded crystals of the starting materials, whereas the 1:2 and 1:4 ratios both gave similar assemblies of the same cocrystal structures.

Physical Properties Measurements. Melting point was measured with a Stuart Scientific Melting Point Apparatus SMP 3. Differential scanning calorimetry (DSC) data were obtained using Perkin Elmer STA600 (40 μL platinum pans, 20–600 °C, heating rate at 10.0 °C/min, Pyris Series software for data processing). Elemental analyzes were carried out by analytical services at the Department of Chemistry, University of Jyväskylä.

Single Crystal X-Ray Measurements. Crystals were measured at 120 K on a Rigaku Oxford Diffraction Supernova diffractometer (Oxford Diffraction, Woodlands, Tex, USA), using Cu Kα (λ = 1.54184 Å) radiation. The CrysAlisPro (Version 1. 171. 39. 43C) package was used for cell refinements and data reductions. Multi-scan (**1**, **2**) or analytical (**3**) absorption corrections (CrystAlisPro, Yarnton, Oxfordshire, England) were applied to the intensities before structure solutions. The structures were solved by the intrinsic phasing method using SHELXT [41]. All structures were refined by using SHELXL program. Crystal data of cocrystal **1**-**3** are listed in Table 1.

Table 1. Crystal data 1–3.

	1	**2**	**3**
Formula moiety	$(C_{10}H_8N_2S)$, $0.5(C_6H_4I_2)$	$2(C_{10}H_8N_2S)$, $3(C_6F_4I_2)$, (CH_2Cl_2)	$(C_{10}H_8N_2S)$, $2(C_6F_5I)$
Empirical formula	$C_{13}H_{10}IN_2S$	$C_{39}H_{18}Cl_2F_{12}I_6N_4S_2$	$C_{22}H_8F_{10}I_2N_2S$
Molecular weight	353.19	1666.99	776.16
Crystal system	Triclinic	Triclinic	Monoclinic
Space group	P-1	P-1	$P2_1/c$
a, Å	7.0677(3)	11.1401(3)	22.6204(3)
b, Å	8.6967(4)	15.9270(4)	8.53950(10)
c, Å	11.1576(5)	16.2566(4)	13.00460(10)
α, °	100.990(4)	63.216(3)	90
β,°	100.380(4)	76.370(2)	103.5430(10)
γ, °	104.057(4)	71.299(2)	90
Volume, Å	634.33(5)	2424.76(13)	2442.21(5)
Z	2	2	4
Density, g/cm^3	1.849	2.283	2.111
T, K	120(2)	120(2)	123(2)
μ (K_α) (mm^{-1})	21.185	32.729	21.895
No. relns.	6446	58,192	16,460
θ Range (°)	4.155-76.751	3.063-76.976	4.02-76.948
Unique reflns.	2649	10,175	5149
GOOF (F^2)	1.056	1.048	1.040
R_{int}	0.0345	0.0488	0.0387
R1($I \geq 2\sigma$)	0.0274	0.0311	0.0262
wR2 ($I \geq 2\sigma$)	0.0744	0.0827	0.0629

Synthesis of 1-(4-bipyridyl)-4-thionpyridine (PTP) Zwitterion. 4-Mercaptopyridine (100 mg) was heated at 67 °C for 16 hours with constant stirring until the color turned to orange-yellow. It was then dissolved in 5 mL of boiling water. Saturated NaOH aqueous solution was added in the solution dropwise until pH 10 was reached. The solution was filtered to remove any particulate matter. The filtrate was extracted with dichloromethane (DCM) (6 × 10 mL). The organic phase from the extraction was reduced to 5 mL in rotary evaporation. The reduced solution was further purified through a chromatography column with acetonitrile as the eluent, followed by drying in vacuum.

The solid, pale greenish yellow PTP was obtained with yield of 16.1%. mp 155.3–157.1 °C. Anal. Calcd for $C_{10}H_8N_2S$: C, 63.82; H, 4.29; N, 14.89. Found: C, 63.62; H, 4.29; N, 14.81. ^{1}H NMR ($CDCl_3$, 300MHz): δ- 8.83 (dd, 2H, J = 4.6), 7.53 (d, 2H, J = 7.4), 7.43 (d, 2H, J = 7.4), 7.34 (dd, 2H, J = 4.6). ^{13}C NMR ($CDCl_3$, 300 MHz): δ- 152.52, 132.21, 131.31, 116.05.

PTP/DIB (1). PTP (5 mg) and 16.5 mg DIB were dissolved in 6 mL DCM in a vial covered with a layer of parafilm and let stand at room temperature. After 3 days, light yellow crystals suitable for single X-ray diffraction were harvested. Anal. Calcd for $C_{13}H_{10}IN_2S$: C, 44.21; H, 2.85; N, 7.93. Found: C, 44.19; H, 2.84; N, 7,91.

PTP/DITFB (2). PTP (5 mg) and 21.5 mg DITFB were dissolved in 6 mL DCM in a vial covered with a layer of parafilm and allowed to stand at room temperature for 5 days. Yellow crystals suitable for single X-ray diffraction were obtained. Anal. Calcd for $C_{39}H_{18}Cl_2F_{12}I_6N_4S_2$: C, 28.08; H, 1.09; N, 3.36. Found: C, 28.08, H, 1.08; N, 3.34.

PTP/IPFB (3). PTP (5 mg) and 15.5 mg IPFB were dissolved in 6 mL DCM in a vial sealed with a layer of parafilm and evaporated at room temperature for a week to obtain greenish yellow crystals suitable for single X-ray diffraction. Anal. Calcd for $C_{28}H_8F_{15}I_3N_2S$: C, 34.04; H, 1.04; N, 3.61. Found: C, 34.09; H, 1.02; N, 3.64.

3. Results

The PTP molecule formed halogen bonded cocrystals with all three XB donors: PTP/DIB (1), PTP/DITFB (2), and PTP/IPFB (3).

The asymmetric unit of **1** contains one complete PTP molecule and half of the DIB molecule. The N-atom in PTP is engaged with one I-atom from DIB forming halogen bond [$d_{N\cdots I}$ 2.968(3)Å and $<_{C\text{-}I\cdots N}$ 177.01°]. In this structure the DIB molecule act as a symmetric ditopic XB donor bridging two PTP molecules through N-atoms. The S-atom of PTP is not involved in XB bonds. Instead it interacts with two neighboring PTP and one nearby DIB via weak C-H···S hydrogen bonds [$d_{S\cdots C5}$ 3.808Å, $<_{C5\text{-}H\cdots S}$ 155.3°; $d_{S\cdots C7}$ 3.795Å, $<_{C7\text{-}H\cdots S}$ 164.97°; $d_{S\cdots C12}$ 3.712Å, $<_{C12\text{-}H\cdots S}$ 136.09°] (Figure 2). Such an arrangement could indicate that the N atom of PTP is favored over S in XB formation.

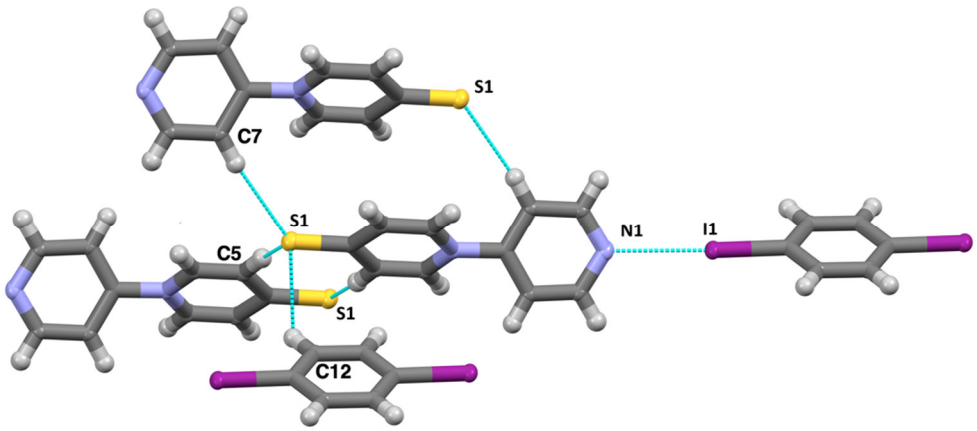

Figure 2. N···I XB and S···H contacts in **1**.

The asymmetric unit of **2** is comprised of two complete PTP molecules, one complete DITFB molecule, four halves of DITFB molecules, and a complete CH_2Cl_2 solvent molecule. In this structure both the S-atom and the N-atom of PTP interact with DITFB molecules by XBs. One DITFB molecule bridges two PTP molecules by N···I halogen bonds [$d_{N2\cdots I1}$ 2.845(6)Å and $<_{C\text{-}I1\cdots N2}$ 171.4(2) °; $d_{N4\cdots I2}$ 2.915(6) and $<_{C\text{-}I2\cdots N4}$ 176.7(2) °]. At the same time the S-atom of PTP also acts as a bifurcated bridging point binding two other DITFB molecules [$d_{S1\cdots I3}$ 3.096(1) and $<_{C\text{-}I3\cdots S1}$ 174.6(1)Å; $d_{S1\cdots I6}$ 3.215 and $<_{C\text{-}I6\cdots S1}$ 171.8(1) °; $d_{S2\cdots I4}$ 3.137(1) and $<_{C\text{-}I4\cdots S2}$ 172.6(1); $d_{S2\cdots I5}$ 3.300(1) and $<_{C\text{-}I5\cdots S2}$ 171.7(1) °], as shown in

Figure 3a. Noticeably, two PTP molecules are connected via S1···H-C [$d_{S1\cdots C}$ 2.929Å, $<_{S1\cdots H\text{-}C}$ 162.89°] and I4 simultaneously connects a neighboring PTP molecule via I4···H3-C3 [$d_{I4\cdots C3}$ 3.927Å, $<_{I4\cdots H3\text{-}C3}$ 136.98°]. The key feature of this structure is that through the I···N and the bifurcated I···S XBs twelve membered rings are formed, giving an expanded wavy 2D network structure with S as the node (Figure 3). Furthermore, 2D networks are connected with adjacent units via F···H, F···C and S···H intermolecular contacts to form a five-folded interpenetrated 3D network. No solvent occupied channels edged by PTP/DITFB are formed.

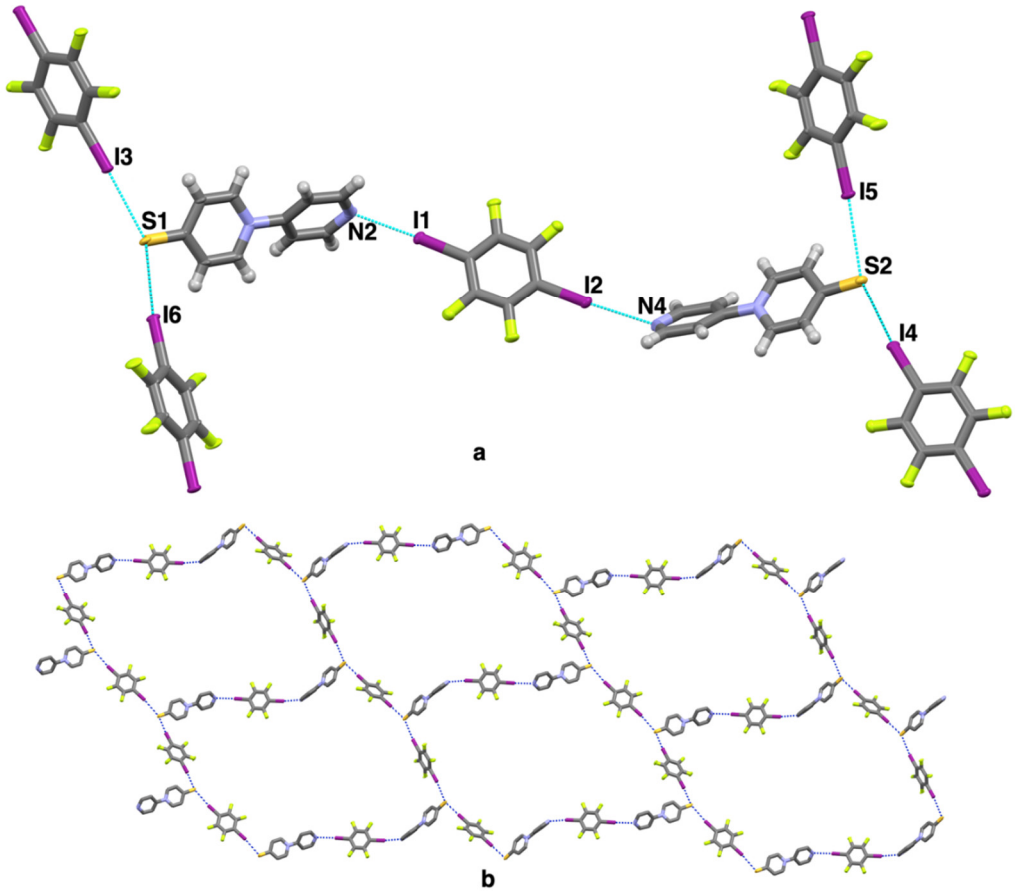

Figure 3. XBs and extended structure of **2**. (**a**) XBs on S and N; (**b**) extended 2D structure of **2**. Solvent CH_2Cl_2 and hydrogen atoms are omitted for clarity.

The asymmetric unit of **3** has one PTP molecule and two IPFB units. XB interactions only take place through the S-atom of PTP, which forms a pair of bifurcated XBs [$d_{S1\cdots I1}$ 3.1224(8)Å and $<_{C\text{-}I1\cdots S1}$ 175.47(7)°; $d_{S2\cdots I2}$ 3.1122(8) and $<_{C\text{-}I2\cdots S1}$ 176.9(1)°]. In this structure the N-atom interacts with two adjacent PTP molecules via weak C-H···N contacts [$d_{N\cdots C}$ 3.423Å, $<_{N\cdots H\text{-}C2}$ 132.55°; $d_{N\cdots C9}$ 3.259Å, $<_{N\cdots H\text{-}C9}$ 117.59°; $d_{N\cdots C10}$ 3.250Å, $<_{N\cdots H\text{-}C10}$ 117.38°] (Figure 4). The relatively large deviation from 180° of all three $<_{N\cdots H\text{-}C}$ is may be affected by the dispersion interactions, which can have an impact on the geometry of HBs in bulky systems [42]. Unlike in **1**, in **3** the XB formation favors I···S interactions. It could indicate that the stronger XB donor IPFB forms XBs with S-atom more easily than iodine in the DIB donor. The structure is further expanded through F···H and S···H contacts.

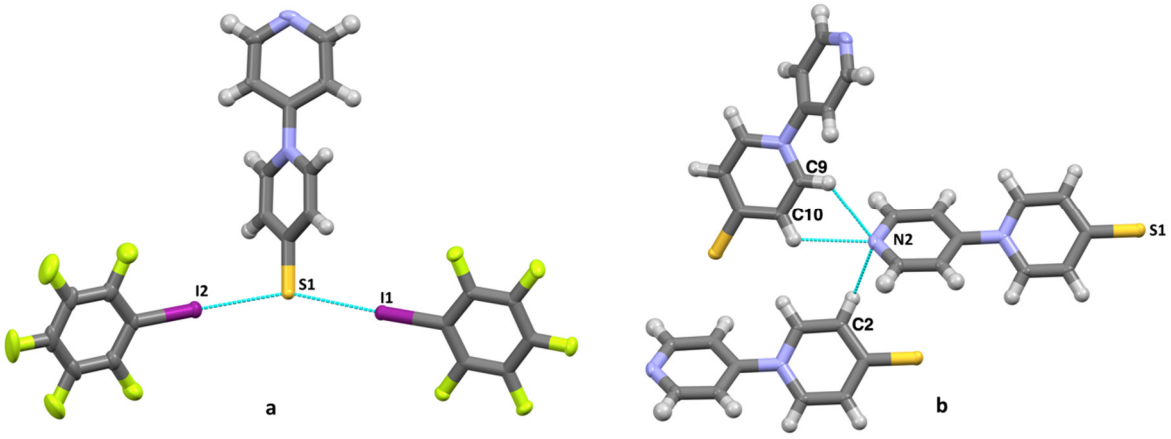

Figure 4. Nonvalent interactions in **3** involving S and N acceptors. (**a**) XBs on S; (**b**) H···N contacts.

Based on the DSC measurements, shown in Table 2, the order of the thermal stability of cocrystals **1–3** are **1** > **2** > **3**. Both **1** and **2** contain I···N halogen bonds. In **3** there are only bifurcated I···S interactions. This could indicate that formation of I···N interactions are stabilizing the structure of the cocrystals. However, it is likely that HBs between XB donor and the S-atom of the acceptor in **1** also play an important role in the overall packing. The results suggest that other type of intermolecular interactions than XBs could be the dominating factors behind the thermal stability in cocrystals 1-3.

Table 2. DSC measurements.

Crystals	T_c /°C
1	127.67
2	114.46
3	85.36

4. Discussion

The relative strength of XB is often described using the halogen bonding interaction ratio, R_{XB}, which is defined as $R_{XB} = d_{XB}/(X_{vdW} + B_{vdW})$ (d_{XB} is the distance between a halogen atom X and the acceptor atom B in Å). Typically, Bondi vdW radii are used for both X_{vdW} and B_{vdW}) [43–48]. A smaller value of R_{XB} indicates stronger XB strength. The key structure parameters of XBs in cocrystal **1–3** are listed in Table 3.

Table 3. Halogen bonds in 1–3.

Crystal*	I···A	d (I···A) Å	<C-I···A °	Symmetry Operations	R_{XB}
1	I···N	2.968(3)	177.01(9)	x, y, z	0.839
2	I1···N2	2.845(6)	171.4(2)	x, y, z	0.806
	I2···N4	2.915(6)	176.7(2)	x, y, z	0.826
	I3···S1	3.096(1)	174.6(1)	1−x, 1−y, 2−z	0.819
	I6···S1	3.215(1)	171.8(1)	1+x, y, z	0.851
	I4···S2	3.137(1)	172.6(1)	−1+x, y, −1+z	0.830
	I5···S2	3.300(1)	171.7(1)	−x, 1−y, 1−z	0.873
3	I1···S1	3.1224(8)	175.47(7)	2−x, 2−y, 1−z	0.826
	I2···S1	3.1122(8)	176.9(1)	1−x, −1/2+y, 1/2−z	0.823

According to this qualitative R_{XB} values, the strongest XB is an I···N contact found in **2**. On the other hand, the weakest contact is an I···S interaction. This time it is found in the second thermally most stable **2**. All in all, the variations in R_{XB} values are quite small and obviously they cannot alone

explain the favored packing patterns. The roles of the other non-covalent interactions, especially hydrogen bonds, are also important forces in determination of the final packing pattern.

The N···I length ranges from 2.845 Å to 2.968 Å in cocrystals **1–3**. To compare these values with other reported N···I distances, a CCDC survey was carried out (C=N, I-C, no organometallic complexes, N and I contact distance <3.53 Å, CSD version 5.41, November 2019). The survey gave a median value of $d_{N\cdots I}$ of 3.050 Å. Thus, the I···N in crystals **1–3** are shorter than most reported ones, indicating a stronger I···N halogen bond. Moreover, R_{XB} of **1** is 0.839, while the R_{XB} of the two I···N in **2** are 0.806 and 0.826, respectively, indicating that both I···N in **2** are stronger than the one found in **1**. Such a result is expected, as the iodine atom in DITFB is more electronegative compared to the corresponding value in DIB due to the fluorine substituents.

To compare the I···S found in cocrystals **2** and **3** with the previously reported sp^3-S contacts, another CCDC survey was performed (C-S and S is in sp^3 hybridization, I-C, no organometallic complexes, S and I contact distance <3.78 Å, CSD version 5.41, November 2019). $d_{I\cdots S}$ in **2** and **3** were in the range of 3.096–3.300 Å, which was shorter than the median of 3.668 Å found from the CCDC survey, indicating again stronger XBs in **2** and **3**. In **2** the average $d_{I\cdots S1}$ was 3.155 Å and the average $d_{I\cdots S2}$ was 3.219 Å, while in **3** the average $d_{I\cdots S1}$ was 3.117 Å. This suggested that I···S interactions in **3** were stronger than in **2**. Such difference in I···S strength is probably due to the fact that iodine is in a stronger electron withdraw environment in IPFB than in DITFB.

Clearly, PTP demonstrates its ability as an acceptor to form strong XBs through both its acceptor atoms. However, both N and S acceptors were not involved in XB interactions in all structures. In **1**, only the N-atom of PTP was acting as a XB acceptor interacting with the DIB, the weakest XB donor used in this study. Whereas in **2** both S-atom and N-atom interact with DITFB, a stronger XB donor than DIB, to form XBs. On the contrary to **1**, in **3** only the S-atom was involved in XB with IPFB, the strongest XB donor in this study. Such a trend could indicate some selectivity in the XB formation. The hard-soft acid-base (HSAB) theory, which gives a plausible explanation for the competition between XB and HB regarding S and N [49], fails to explain the XB selectivity in **1–3**, because the I-atom in IPFB, the hardest I-atom compared with that in DIB and DITFB due to the strongest polarization caused by F substitutions, chooses the soft S instead of the hard N. However, though I-atom in IPFB is the hardest among the three XB donors, it is still soft in nature, especially when compared to N. Thus, the apparent selectivity can be influenced by other noncovalent interactions. To estimate the contribution of XB to the total molecular interactions in **1–3**, Hirshfeld surface analyses was used, which is a method to analyze the interactions in molecular packing and comparison of crystal structures [50,51]. CrystalExplorer 17.5 [52] was used to create Hirshfeld surfaces around PTP in **1–3** in Figure 5. The contribution of XB to the Hirshfeld surface of each crystal structure is summarized in Table 4.

Table 4. Contributions of XBs to Hirshfeld surfaces in **1–3.**

Cocrystal	XB	Contribution/%
1	N···I	2.1
2	N···I	3.2
2	S···I	3.4
3	S···I	5.2

The difference in intensity in these fingerprints reveals the difference in XB bond length in the obtained cocrystals; the increase in intensity around *di*/*de*≈1.2 Å/1.65 Å in N···I of **2** compared to that of **1** shows that N···I in **2** is shorter than in **1**. Similarly, the increased intensity around *di*/*de*≈1.5 Å/1.7 Å in I···S of **3** compared to that of **2** arises from the much shorter S···I in **3**. Moreover, the different fingerprint patterns also reveal that the PTP molecule is in different immediate polymorph environment in **1–3** [51]. Fingerprints plot with HB contacts highlighted (supplementary material Figure S6.) illustrate each type of HB contacts with distinctive patterns. The strongest intensities can be found around *di*/*de* ≈1.0-1.2 Å/1.4-2.4 Å region. S···H in **1** has strong intensity around *di*/*de*≈1.1 Å/1.8 Å, while in **2** the strongest region is *di*/*de*≈1.2 Å/1.9 Å. The F···H in **2**, compared with that in 3, reaches a shorter *di* region and has weaker intensity around *di*/*de* ≈1.2 Å/1.4 Å. Moreover, the I···H in

2 demonstrates the strongest interactions around *di*/*de*≈1.2 Å/2.1 Å. Noticeably, the same type of HB contact in different cocrystals has different fingerprints patterns, due to the sensitivity of fingerprints plot to the environment surrounding PTP molecules [51]. Based on the analysis, the XB contribution to the Hirshfeld surface is small, less than 10% in all three cocrystals, indicating that XB is not the prominent crystal stabilizing force. The DSC results yield similar conclusions as well; the weakest XB donor forms the most thermally stable crystal, while the strongest XB donor yields the most thermally unstable one, suggesting other types of intermolecular interactions play more pivotal roles in these crystal structures.

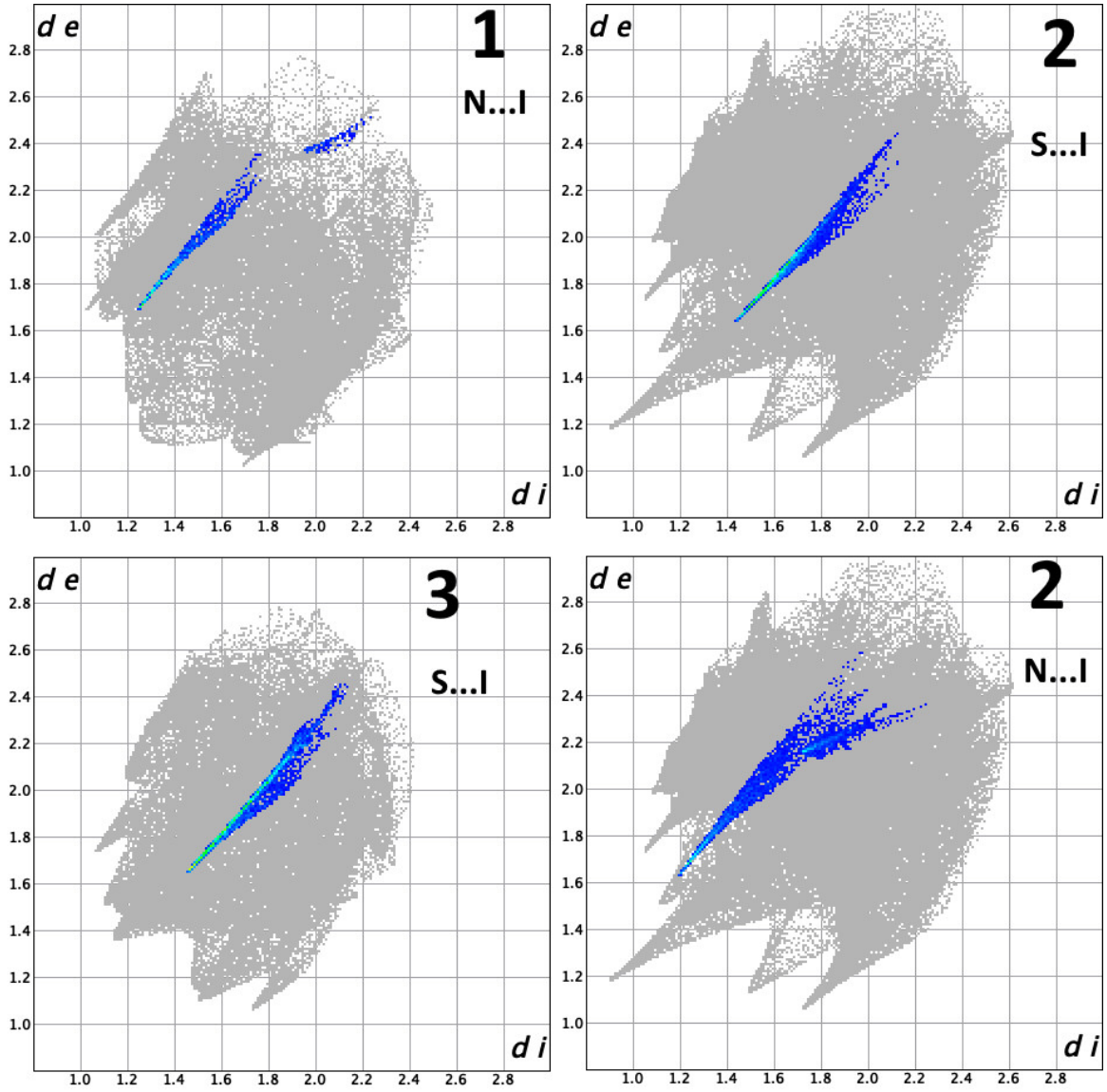

Figure 5. 2D fingerprint plots resolved into N···I in 1, S···I and N···I in 2, and S···I in 3. The full fingerprints appear in each plot as grey.

5. Conclusions

Bidentate, neutral 1-(4-pyridyl)-4-thiopryine (PTP), was synthesized and used as a XB acceptor in this study. Three cocrystals were obtained with comparatively strong XBs, showing that PTP is capable of forming robust XBs. Moreover, with DITFB as the XB donor, PTP demonstrated its ability to form bifurcated XBs on S and single XBs on N simultaneously, generating wavy continuous network structures. The analysis of XBs, together with the Hirshfeld surface analyses and DSC measurements, indicates that the formation of halogen bonds is not necessarily the dominating driving force in the formation of cocrystals. Other non-covalent interactions play key roles in the

final arrangement of molecules. In order to build systematic supramolecular constructions, all intermolecular interactions must always be considered. It is challenging to predict what types of intermolecular interactions will be the dominate ones and this hampers the prediction of non-covalent assemblies.

Supplementary Materials: The following are available online at www.mdpi.com/xxx/s1, Table S1: Descriptive statistics of CCDC survey of sp^2-N, Table S2: Descriptive statistics of CCDC survey of sp^3-S, Figure S1: TGA/DSC spectrum of cocrystal 1, Figure S2: TGA/DSC measurements of cocrystal 2, Figure S3: TGA/DSC spectrum of cocrystal 3, Figure S4: ^{1}H NMR of PTP, Figure S5: ^{13}C NMR of PTP, Figure S6: 2D fingerprints plot resolved in S···H in 1, F···H, S···H and I···H in 2, F···H and N···H in 3. The crystallographic data can also be obtained free of charge in *cif* format by request from the Cambridge Crystallographic Data Centre at www.ccdc.cam.ac.uk/data_request/cif. The CCDC numbers of compounds 1-3 are 982538, 1982539, and 1982540 respectively.

Author Contributions: Synthesis, initial X-ray structure characterization and draft preparation: X.D.; X-structure characterization: M.T.; project planning, supervision, funding acquisition and project administration, manuscript review and editing: M.H. All authors have read and agreed to the published version of the manuscript.

Funding: This research was funded by Academy of Finland, grant number 130571 and 295881.

Conflicts of Interest: The authors declare no conflict of interest.

References

1. Desiraju, G. R.; Ho, P. S.; Kloo, L.; Legon, A. C.; Marquard, R.; Metrangolo, P.; Politzer, P.; Resnati, G.; Rissanen, K. Definition of the Halogen Bond (IUPAC Recommendations 2013). *Pure Appl. Chem*., **2013**, *85*, 1711–1713.
2. Forni, A.; Franchini, D.; Dapiaggi, F.; Pieraccini, S.; Sironi, M.; Scilabra, P.; Pilati, T.; Petko, K.; Resnati, G.; Yagupolkii, Y. L. Featuring I…N Halogen Bond and Weaker Interactions in Iodoperfluoroalkylimidazoles: An Experimental and Theoretical Charge Density Study. *Cryst. Growth Des*. **2019**, *19*, 1621–1631.
3. Awwadi, F. F.; Willett, R. D.; Peterson, K. A.; Twamley, B. The Nature of Halogen···Halides Synthons: Theoretical and Crystallographic Studies. *J. Phys. Chem. A* **2007**, *111*, 2319–2328.
4. Awwadi, F. F.; Taher, D.; Haddad, S. F. Turnbull, M. M. Competition between Hydrogen and Halogen Bonding Interactions: Theoretical and Crystallographic Studies. *Cryst. Growth Des.* **2014**, *14*, 1961–1971.
5. Stilinovi ć, V.; Horvat, G.; Hrenar, T.; Nemec, V.; Cinčić, D. Halogen and Hydrogen Bonding between (N-Halogeno-)-succinimides and Pyridine Derivatives in Solution, the Solid State and In Silico. *Chem. Eur. J.* **2017**, 23, 5244–5257.
6. Politzer, P.; Murray, J. S.; Clark, T. Halogen Bonding: An Electrostatcially-Driven Highly Directional Noncovalent Interaction. *Phys. Chem. Chem. Phys.* **2010**, 12, 7748-7757.
7. Priimagi, A.; Cavallo, G.; Metrangolo, P.; Resntai, G. The Halogen Bond in the Design of Functional Supramolecular Materials: Recent Advances. *Acc. Chem. Res.* **2013**, 46, 11, 2686-2695.
8. Clark, T. Halogen bonds and σ-holes. *Faraday Discuss.*, 2017, *203*, 9–27.
9. Rowe, R. K.; Ho, P. S. Relationships between Hydrogen Bonds and Halogen Bonds in Biological Systems. *Acta Cryst.* **2017**, *B73*, 255–264.
10. Gunawardana, C. A.; Desper, J.; Sinha, A. S.; Đaković, M.; Aakeröy, C. B. Competition and Selectivity in Supramolecular Synthesis: Structural Landscape around 1-(Pyridylmethyl)-2,2′-biimidazoles. *Faraday Discuss.* **2017**, *203*, 371–388.
11. Pfrunder, M. C.; Brock, A. J.; Brown, J. J.; Grosjean, A.; Ward, J.; McMurtrie, J. C.; Clegg, J. J. A Three-dimensional Cubic Halogen-bonded Network. *Chem. Commun*., **2018**, *54*, 3874–3976.
12. Ding, X.; Tuikka, M. J.; Hirva, P.; Kukushkin, V. Y.; Novikov, A. S.; Haukka, M. Fine-tuning Halogen Bonding Properties of Diiodine through Halogen-halogen Charge Transfer-Extended [Ru(2,2′-bipyridine)$(CO)_2X_2$]•I_2 Systems (X=Cl, Br, I). *Cryst. Eng. Comm*. **2016**, *18*, 1987–1995.
13. Pfrunder, M. C.; Micallef, A. S.; Rintoul, L.; Arnold, D. P.; McMurtrie, J. Interplay between the Supramolecular Motifs of Polypyridyl Metal Complexes and Halogen Bond Networks in Cocrystals. *Cryst. Growth Des.* **2016**, *16*, 681–695.
14. Chan, Y-C.; Yeung, Y-Y. Halogen Bond Catalyzed Bromocarbocyclization. *Angew. Chem. Int. Ed.* **2018**, 57, 3483-3487.

15. Carreras, L.; Serrano-Torné, M.; van Leeuwen, P. W. N. M.; Vidal-Ferran, A. XBpos-Rh: A Halogen-bond Assembled Supramolecular Catalyst. *Chem. Sci.*, **2018**, *9*, 3644–3648.
16. Lim, J. Y. C.; Marques, I.; Félix, V.; Beer, P. D. Enantioselective Anion Recognition by Chiral Halogen-Bonding [2]Rotaxanes. *J. Am. Chem. Soc.* **2017**, *139*, 12228–12239.
17. Cavallo, G.; Metrangolo, P.; Milani, R.; Pilati, T.; Priimagi, A.; Resnati, G.; Terraneo. The Halogen Bond. *Chem.Rev.* **2016**, 116, 2478–2601.
18. Riel, A. M. S.; Decato, D. A.; Sun, J.; Massena, C. J.; Jessop, M. J.; Berryman, O. B. The Intramolecular Hydrogen Bonded-halogen Bond: A New Strategy for Preorganization and Enhanced Binding. *Chem. Sci.*, **2018**, *9*, 5828–5836.
19. Dichiarante, V.; Kaiho, T.; Metrangolo, P.; Pilati, T.; Resnati, G.; Terraneo, G.; Ursini, M. The Diiodomethyl-sulfonyl Moiety: An Unexplored Halogen Bond-donor Motif. *Chem. Commun.* **2019**, *55*, 4234–4237.
20. Carletta, A.; Zbačnik, M.; Vitković, M.; Tumanov, N.; Stilinović, V.; Wouters, J.; Cinčić, D. Halogen-bonded Cocrystals of N-salicylidene Schiff Bases and Iodoperfluorinated Benzenes: Hydroxyl Oxgen as A Halogen Bond Acceptor. *Cryst. Eng. Comm*. **2018**, *20*, 5332–5339.
21. Zbačnik, M.; Vitković, M.; Vulić, V.; Nogalo, I.; Cinčić, D. Competiton between Halogen Bonds in Cocrystals of Imines Derived from *o*-Vanillin. *Cryst. Growth Des.* **2016**, *16*, 6381–6389.
22. Carletta, A.; Zbačnik, M.; Gysel. M. V.; Vitković, M.; Tumanov, N.; Stilinović, Wouters, J.; Cinčić. Playing with Isomerism: Cocrystallization of Isomeric N-Salicylideneaminopyridines with Perfluorinated Compounds as Halogen Bond Donors and Its Impact on Photochromism. *Cryst. Growth Des.* **2018**, *18*, 6833–6842.
23. Koskinen, L.; Jääskeläiinen, S.; Hirva, P.; Haukka; M. Tunnable Interaction Strength and Nature of the S···Br Halogen Bonds in [(Thione)Br_2] Systems. *Cryst. Growth Des.* **2015,** 15, 1160-1167.
24. Koskinen, L.; Hirva, P.; Hasu, A.; Jääskeläinen, S.; Koivistoinen, J.; Petterson, M.; Haukka, M. Modification of the Supramolecular Structure of [(Thione)IY] (Y=Cl, Br) Systems by Cooperation of Strong Halogen Bonds and Hydrogen Bonds. *Cryst. Eng. Comm*. **2015**, *17*, 2718–2727.
25. Eccles, K. S.; Morrison, R. E.; Sinha, A. S.; Maguire, A. R.; Lawrence, S. E. Investigating C=S···I Halogen Bonding for Cocrystallization with Primary Thionamides. *Cryst. Growth Des*. **2015**, *15*, 3442–3451.
26. Le Gal, Y.; Lorcy, D.; Jeannin, O.; Barrière, F.; Dorcet, V.; Lieffrig, J.; Fourmigué, M. C=S···I Halogen Bonding Interactions in Crystalline Iodinated Dithiole-2-thiones and Thiazole-2-thiones. *Cryst. Eng. Comm*. **2016**, *8*. 5474–5481.
27. Cauliez, P.; Polo, V.; Roisnel, T.; Llusar, R.; Fourmigué. The Thiocyanate anion as a polydentate halogen bond acceptor. *Cryst. Eng. Comm*. **2010**, *12*, 558–556.
28. Cinčić, D.; Friščić, T.; Joens, W. Experimental and Database Studies of Three-centered Halogen Bonds with Bifurcated Acceptors Present in Molecular Crystals, Cocrystals and Salts. *Cryst. Eng. Comm*. **2011**, *13*, 3224–3231.
29. Goud, N. R.; Bolton, O.; Burgess, E. C.; Matzger. A.J. Unprecedented Size of the σ-Holes on 1,3,5-Triiodo-2,4,6-trinitrobenzene Begets Unprecedented Intermolecular Interactions. *Cryst. Growth Des.* **2016**, *16*, 1765–1771.
30. Pigge, F. C.; Kapadia, P. P.; Swenson, D.C. Halogen Bonded Networks from Pryidyl-substituted Tetraarylethylenes and Diiodotetrafluorobenzenes. *Cryst.Eng. Comm*. **2013**, *15*, 4386–4391.
31. Ravat, P.; Lekshmi, S. S.; Biswas, S. N.; Nandy, P.; Varughese, S. Equivalence of Ethylene and Azo-Bridges in the Modular Design of Molecular Complexes: Role of Weak Interactions. *Cryst. Growth Des.* **2015**, *15*, 2389–2401.
32. Aakeröy, C. B.; Spartz, C. L.; Dembowski, S.; Dwyre, S.; Desper, J. A Systematic Structural Study of Halogen Bonding *versus* Hydrogen Bonding within Competitive Supramolecular Systems. *IUCrJ*. **2015**, *2*, 498–510.
33. Bosch, E.; Kruse, S. J.; Groeneman, R. H. Infinite and Discrete Halogen Bonded Assemblies Based upon 1, 2-Bis(iodoethynyl)benzene. *Cryst. Eng. Comm*. **2019**, *21*, 990–993.
34. Peterson, A.; Kaasik, M.; Metsala, A.; Järving, I.; Adamson, J.; Kanger, T. Tunable chiral triazole-based halogen bond donors: assessment of donor strength in solution with nitrogen-containing acceptors. *RSC Adv*., **2019**, *9*, 11718–11721.

35. Lee, S.; Chen, B.; Fredrickson, D. C.; DiSalvo, F. J.; Lobkovsky, E.; Adams, J. Crystal Structures of (Pyrene)$_{10}$(I_3^-)$_4$(I_2)$_{10}$ and [1, 3, 6, 8-Tetrakis(methylthio)pyrene]$_3$(I_3^-)$_3$(I_2)$_7$: Structural Trends in Fused Aromatic Polyiodides. *Chem. Mater.* **2003**, *15*, 1420–1433.
36. Tamilselvi, A.; Mugesh, G. Interaction of Heterocyclic thiols/thiones eliminated from cephalosporins with iodine and its biological implications. *Bioorg. Med. Chem. Lett.* **2010**, *20* 3692–3697.
37. Mancini, A.; Pala, L.; Aragoni, M. C.; Arca. M.; Devillanova, F. A.; Hursthouse, M. B.; Light, M. E.; Skabara, P. J.; Bricklebank, N. Structural and DFT Studies of Dibromine and Diiodine Adducts of a Sulfur-Rich Thiocarbonyl Donor. *Eur. J. Inorg. Chem.* **2012**, 2373–2380; doi:10.1002/ejic.201101028
38. Eichstaedt, K.; Wasilewska, A.; Wicher, B.; Gdaniec, M.; Połoński. Supramolecular Synthesis Based on a Combination of Se···N Secondary Bonding Interactions with Hydrogen and Halogen Bonds. *Cryst. Growth Des.* **2016**, *16*, 1282–1293.
39. Montis, R.; Arca, M.; Aragoni, M. C.; Bauzá, A.; Demartin, F.; Frontera, A.; Isaia, F.; Lippolis, V. Hydrogen- and Halogen-bond Cooperativity in Determining the Crystal Packing of Dihalogen Charge-transfer Adducts: A Study Case from Heterocyclic Pentatomic Chalcogenone Donors. *Cryst. Eng. Comm.* **2017**, *19*, 4401–4412.
40. Ivolgina, V. A.; Chernov'yants, M. S.; Popov, L. D.; Suslonov, V. V.; Borodkin, G. S.; Luanguzov, N. V.; Avtushenko, N. A. Perspective Anti-thyroid Druy 2-thioxo-5-(3, 4, 5-trimethoxybenzylidene) thiazolidine-4-one: X-ray and Thermogravimetric Characterization of Two Novel Molecular Adducts, Obtained by Interaction with I_2. *J. Mol. Struct*. **2019**, *1180*, 629–635.
41. Sheldrick, G. M. Crystal Structure Refinement with SHELXL. *Acta Cryst*. **2015**, *C71*, 3–8.
42. Van der Lubbe, S. C. C.; Guerra, C. F. The Nature of Hydrogen Bonds: A Delineation of the Role of Different Energy Components on Hydrogen Bond Strengths and Lengths. *Chem. Asian J.* **2019**, *14*, 2760–2769.
43. Bondi, A. van der Waals Volumes and Radii. *J. Phys. Chem.* **1964**, *68*, 441–451.
44. Lommerse, P. M.; Stone, A. J.; Taylor, R.; Allen, F.H. The Nature and Geometry of Intermolecular Interactions Between Halogen and Oxygen or Nitrogen. *J. Am. Chem. Soc*. **1996**, *118*, 3108–3116.
45. Brammer, L.; Bruton, E. A.; Sherwood, P. Understanding the Behavior of Halogens as Hydrogen Bond Acceptors. *Cryst. Growth Des*. **2001**, *1*, 277–290.
46. Zordan, F.; Brammer, L.; Sherwood, P. Supramolecular Chemistry of Halogens: Complementary Features of Inorganic (M-X) and Organic (C-X') halogens Applied to M-X···X'-C Halogen Bond Formation. *J. Am. Chem. Soc.* **2005**, *127*, 5979–5989.
47. Johnson, M. T.; Džolić, Z.; Cetina, M.; Wendt, O. F.; Öhrström, L.; Rissanen, K. Neutral Organometallic Halogen Bond Acceptors: Halogen Bonding in Complexes of PCPPdX (X=Cl, Br, I) with Iodine (I_2), 1,4-Diiodotetrafluorobenzene (F4DIBz), and 1,4-Diiodooctafluorobutane (F8DIBu). *Cryst. Growth Des.* **2012**, *12*, 362–368.
48. Ding, X.; Tuikka, M.; Rissanen, K.; Haukka, M. Extended Assemblies of Ru(bpy)$(CO)_2X_2$ (X=Cl, Br, I) Molecules Linked by 1,4-Diiodotetrafluoro-Benzene (DITFB) Halogen Bond Donors. *Crystals*. **2019**, *9*, 319.
49. Riel, A. M. S.; Jessop, M. J.; Decato, D. A.; Massena, C. J.; Nascimento, V. R.; Berryman, O. B. Experimental Investigation of Halogen-bond Hard-soft Acid-base Complementarity. *Acta Cryst*. **2017**, *B73*, 203–209.
50. Spackman, M. A.; Jayatilaka, D. Hirshfeld Surface Analysis. CrystEngComm, **2009**, *11*, 19–32.
51. Yang, P.; Qin C.; Du, S.; Jia, L.; Qin, Y.; Gong J.; Wu, S.Crystal Structure, Stability and Desolvation of the Solvates of Sorafenib Tosylate. *Crystals*. **2019**, *9*, 367.
52. Turner, M. J.; McKinnon, J. J.; Wolff, S. K.; Grimwood, D. J.; Spackman, M. A. CrystalExplorer Model Energies and Ergy Frameworks: Extension to Metal Coordination Compounds, Organic Salts, Solvates and Open-shell Systems. *ICUrJ*. **2017**, *4*, 547–587.